
Article:
Tremblay, P-E., Gentile-Fusillo, N., Raddi, R. et al. (9 more authors) (2017) The Gaia DR1 mass–radius relation for white dwarfs. Monthly Notices of the Royal Astronomical Society, 465 (3). pp. 2849-2861. ISSN 0035-8711

https://doi.org/10.1093/mnras/stw2854

MNRAS **000**, 1–13 (2016) Preprint 3 November 2016 Compiled using MNRAS LATEX style file v3.0

The Gaia DR1 Mass-Radius Relation for White Dwarfs

P.-E. Tremblay[1⋆], N. Gentile-Fusillo[1], R. Raddi[1], S. Jordan[2], C. Besson[3], B. T. Gänsicke[1], S. G. Parsons[4], D. Koester[5], T. Marsh[1], R. Bohlin[6], J. Kalirai[6]

[1]*Department of Physics, University of Warwick, CV4 7AL, Coventry, UK*
[2]*Astronomisches Rechen-Institut, Zentrum für Astronomie der Universität Heidelberg, D-69120 Heidelberg, Germany*
[3]*Arts et Métiers ParisTech Centre de Bordeaux-Talence, Esplanade des Arts et Métiers, 33400 Talence, France*
[4]*Department of Physics and Astronomy, University of Sheffield, S3 7RH, Sheffield, UK*
[5]*Institut für Theoretische Physik und Astrophysik, Universität Kiel, D-24098 Kiel, Germany*
[6]*Space Telescope Science Institute, 3700 San Martin Drive, Baltimore, MD 21218, USA*

Accepted XXX. Received YYY; in original form ZZZ

ABSTRACT

The *Gaia* Data Release 1 (DR1) sample of white dwarf parallaxes is presented, including 6 directly observed degenerates and 46 white dwarfs in wide binaries. This data set is combined with spectroscopic atmospheric parameters to study the white dwarf mass-radius relationship (MRR). *Gaia* parallaxes and *G* magnitudes are used to derive model atmosphere dependent white dwarf radii, which can then be compared to the predictions of a theoretical MRR. We find a good agreement between *Gaia* DR1 parallaxes, published effective temperatures ($T_{\rm eff}$) and surface gravities ($\log g$), and theoretical MRRs. As it was the case for *Hipparcos*, the precision of the data does not allow for the characterisation of hydrogen envelope masses. The uncertainties on the spectroscopic atmospheric parameters are found to dominate the error budget and current error estimates for well-known and bright white dwarfs may be slightly optimistic. With the much larger *Gaia* DR2 white dwarf sample it will be possible to explore the MRR over a much wider range of mass, $T_{\rm eff}$, and spectral types.

Key words: white dwarfs – stars: fundamental parameters – stars: interiors – parallaxes – stars: distances

1 INTRODUCTION

The white dwarf mass-radius relationship (MRR) is fundamental to many aspects of astrophysics. At one end of the spectrum, the upper mass limit first derived by Chandrasekhar (1931) is the central basis of our understanding of type Ia supernovae, standard candles that can be used to measure the expansion of the Universe (Riess et al. 1998; Perlmutter et al. 1999). On the other hand, the MRR is an essential ingredient to compute white dwarf masses from spectroscopy, photometry, or gravitational redshift measurements (see, e.g., Koester et al. 1979; Shipman 1979; Koester 1987; Bergeron et al. 1992, 2001; Falcon et al. 2012). These masses calibrate the semi-empirical initial to final mass relation for white dwarfs in clusters and wide binaries (see, e.g., Weidemann 2000; Catalán et al. 2008; Kalirai et al. 2008; Williams et al. 2009; Casewell et al. 2009; Dobbie et al. 2012; Cummings et al. 2016). These results unlock the potential for white dwarfs to be used to understand the chemical evolution of galaxies (Kalirai et al. 2014), date old stellar populations (Hansen et al. 2007; Kalirai 2012), and trace the local star formation history (Tremblay et al. 2014).

On the theoretical side, the first MRRs that were utilized assumed a zero temperature fully degenerate core (Hamada & Salpeter 1961). The predictions have now improved to include the finite temperature of C and O nuclei in the interior and the non-degenerate upper layers of He and H (Wood 1995; Hansen 1999; Fontaine et al. 2001; Salaris et al. 2010; Althaus et al. 2010a). The MRRs were also extended to lower and higher mass ranges, with calculations for He and O/Ne cores, respectively (Althaus et al. 2007, 2013). The total mass of the gravitationally stratified H, He, and C/O layers in white dwarfs is poorly constrained since we can only see the top layer from the outside. While there are some constraints on the interior structure of white dwarfs from asteroseismology (Fontaine et al. 1992; Romero et al. 2012, 2013; Giammichele et al. 2016), the white dwarf cooling sequence in clusters (Hansen et al. 2015; Goldsbury et al. 2016), and convective mixing studies (Sion 1984; Tremblay & Bergeron 2008; Bergeron et al. 2011), a theoretical MRR assuming a specific interior stratification is usually preferred (Iben & Tutukov 1984; Fontaine et al. 2001; Althaus et al. 2010b). For hydrogen-atmosphere DA white dwarfs, most studies assume thick hydrogen layers with $q_{\rm H} = M_{\rm H}/M_{\rm tot} = 10^{-4}$, which is an estimate of the maximum hydrogen mass for residual nuclear burning (Iben & Tutukov 1984). More detailed calculations for the maximum H envelope mass as a function of the white dwarf mass have also been employed (Althaus et al. 2010b). On the other hand, thin H-layers ($q_{\rm H} = 10^{-10}$) are often used for helium

⋆ E-mail: P-E.Tremblay@warwick.ac.uk

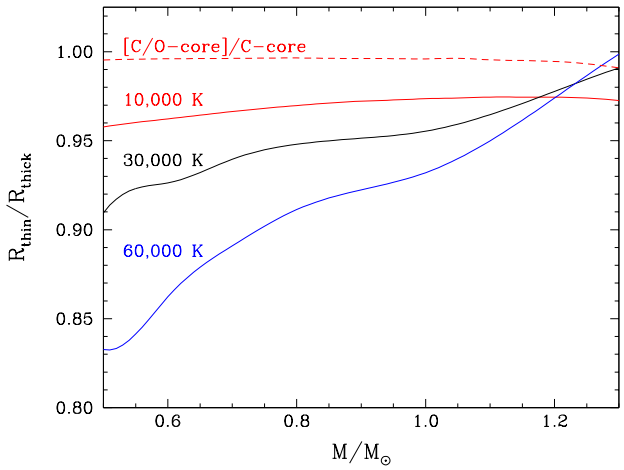

Figure 1. Ratio of the predicted radii for thick ($q_{\rm H} = 10^{-4}$) and thin ($q_{\rm H} = 10^{-10}$) hydrogen layers as a function of the white dwarf mass. Cooling sequences from Fontaine et al. (2001) at $T_{\rm eff}$ = 10,000 K (solid red line) and 30,000 K (black), as well as the models of Wood (1995) at 60,000 K (blue) were employed. We also show the difference between the C/O-core (50/50 by mass fraction mixed uniformly) and pure-C cooling tracks at 10,000 K (dashed red line).

atmospheres (DB, DZ, DQ, and DC). Fig. 1 demonstrates that the MRR varies by 1–15%, depending on the white dwarf mass and temperature, whether a thick or a thin hydrogen layer is assumed. As a consequence, an observed MRR that would achieve a 1%-level precision could in principle constrain the layering of white dwarfs. On the other hand, Fig. 1 shows that the effect of varying the C/O ratio in the core is very small on the MRR (< 1%).

Despite its fundamental importance, the MRR of white dwarfs is not robustly constrained by observations. One of the most successful tests so far has been from eclipsing binaries including a white dwarf. Currently, this method can reach a precision of ∼2% on the MRR (Parsons et al. 2016). These derivations are based on photometric observations of the eclipses and kinematic parameters, and are almost completely independent of white dwarf model atmospheres. The disadvantage is that there are only a few known such systems (O'Brien et al. 2001; Parsons et al. 2010; Pyrzas et al. 2012; Parsons et al. 2012a,b,c; Bours et al. 2015; Parsons et al. 2016) and their configuration implies that they are always post-common envelope binaries that have previously interacted.

Another method to test the MRR is to rely on astrometric binaries with known distances and precise dynamical orbital mass measurements (Shipman et al. 1997; Barstow et al. 2005; Bond et al. 2015). There are only a few such systems, with Sirius, 40 Eri, and Procyon being the most studied. One can then use the observed gravitational redshift, e.g. from the wavelength shift of the cores of the Balmer lines, to derive the radius of the white dwarf relatively independently of its atmospheric parameters. For the case of Sirius B, the gravitational redshift measurements are still not fully understood and more work is needed to comprehend all constraints on mass and radius (Barstow et al. 2005, 2015). Nevertheless, high-resolution and high signal-to-noise spectroscopic observations allow for radial velocity measurements at a ∼2.5% precision level (Zuckerman et al. 2013), highlighting the potential of this technique.

All other methods to derive the MRR are semi-empirical and rely on the atmospheric parameters, the effective temperature ($T_{\rm eff}$) and surface gravity ($\log g$). The latter are most often constrained by comparing detailed model spectra to the observed Balmer lines in DA white dwarfs (Bergeron et al. 1992; Finley & Koester 1997) and to the He I lines in DB white dwarfs (Bergeron et al. 2011; Koester & Kepler 2015). If a dynamical mass is available, one can then derive the radius from the spectroscopic surface gravity, but for most white dwarfs it is not possible.

The calculation of the semi-empirical MRR using atmospheric parameters was pioneered by Schmidt (1996) and Vauclair et al. (1997) with trigonometric parallax measurements for 20 white dwarfs directly observed from the *Hipparcos* satellite. This technique was later expanded to include wide binary systems for which the primary has a precise *Hipparcos* parallax (Provencal et al. 1998; Holberg et al. 2012). This method is based on the fact that the energy flux measured at the earth is R^2/D^2 times the flux emitted at the surface of the star, where R is the stellar radius and D the distance to earth. The flux emitted at the surface itself depends on the predictions from model atmospheres. The atmospheric parameters coupled with the distance can therefore allow for the derivation of a semi-empirical radius. As highlighted by Vauclair et al. (1997), once the surface flux is integrated and observed over a broad photometric band, the derived radius depends almost only on $T_{\rm eff}$ and very little on $\log g$. One can then compute a mass independent of the MRR by using the radius defined above and the spectroscopic $\log g$.

Given that the atmospheric parameters are employed to derive the semi-empirical MRR, it is not straightforward to disentangle a genuine signature of a MRR and interior structure from systematic model atmosphere effects. We note that some authors have actually *assumed* a theoretical MRR and used the technique described above to test the accuracy of the atmospheric parameters and model atmospheres (see, e.g., Tremblay et al. 2013). To complicate matters even more, there is a partial degeneracy since increasing both $T_{\rm eff}$ and $\log g$ can result in the same predicted luminosity and distance (Tremblay & Bergeron 2009).

Despite the fact that modern ground-based techniques have achieved a ∼0.5 milliarcsec (mas) precision for parallaxes of a few selected white dwarfs in the solar neighborhood (Harris et al. 2007; Subasavage et al. 2009), the picture of the semi-empirical MRR has remained largely unchanged since the *Hipparcos* study of Vauclair et al. (1997) and the follow-up by Holberg et al. (2012). Vauclair et al. (1997) found that the *Hipparcos* MRR is largely consistent with theoretical predictions when realistic uncertainties on the atmospheric parameters are taken into account. They concluded that the error bars on the atmospheric parameters published in the literature at the time were slightly too optimistic, and that the determination of the size of the H-layers for *Hipparcos* white dwarfs was out of reach.

The main goal of this work is to use *Gaia* DR1 parallaxes for the *Hipparcos* and Tycho-2 catalog white dwarfs, both directly observed and in wide binaries, to re-asses the semi-empirical MRR for degenerate stars. In preparation for future *Gaia* data releases, we want to understand whether it is possible to disentangle uncertainties in the spectroscopic technique from a genuine offset between the theoretical and observed MRRs. Our study is constructed as follows. First we introduce in Section 2 the *Gaia* DR1 and *Hipparcos* white dwarf samples and determine the atmospheric parameters of these objects. We derive the semi-empirical MRR in Section 3 and discuss the implications in Section 4. We conclude in Section 5.

2 THE GAIA DR1 SAMPLE

The European Space Agency (ESA) astrometric mission *Gaia* is the successor of the *Hipparcos* mission and increases by orders of magnitude the precision and number of sources. *Gaia* will determine positions, parallaxes, and proper motions for ∼1% of the stars in the Galaxy, and the catalog will be complete for the full sky for V $\lesssim$ 20 mag (Perryman et al. 2001). The final data release will include between 250,000 and 500,000 white dwarfs, and among those 95% will have a parallax precision better than 10% (Torres et al. 2005; Carrasco et al. 2014). The final catalog will also include *G* passband photometry, low-resolution spectrophotometry in the blue (BP, 330–680 nm) and red (RP, 640–1000 nm), and (for bright stars, $G \lesssim 15$) higher-resolution spectroscopy in the region of the Ca triplet around 860 nm with the Radial Velocity Spectrometer (Jordi et al. 2010; Carrasco et al. 2014).

The *Gaia* DR1 is limited to *G* passband photometry and the five-parameter astrometric solution for stars in common with the *Hipparcos* and Tycho-2 catalogs (Michalik et al. 2014, 2015; Lindegren et al. 2016; Gaia Collaboration 2016). However, not all *Hipparcos* and Tycho-2 stars are found in *Gaia* DR1 owing to source filtering. In particular, sources with extremely blue or red colours do not appear in the catalog (Gaia Collaboration 2016). Unfortunately, this significantly reduces the size of the *Gaia* DR1 white dwarf sample, with most of the bright and close single degenerates missing.

We have cross-matched the *Hipparcos* and Tycho-2 catalogs with Simbad as well as the White Dwarf Catalog (McCook & Sion 1999). A search radius of 10″ around the reference coordinates was employed and all objects classified as white dwarfs were looked at manually. Our method eliminates all objects that are not known to be white dwarfs and wide binaries for which the stellar remnant is at a separation larger than ∼10″ to the *Hipparcos* or Tycho-2 star. We have identified 25 white dwarfs for which the bright degenerate star itself is part of the *Hipparcos* (22 objects) or Tycho-2 (3 objects) catalogs. Those objects are shown in Table 1 with *V* magnitudes along with *Hipparcos* parallax values from van Leeuwen (2007) or alternative ground measurements if available in the literature. The sample includes all *Hipparcos* white dwarfs studied by Vauclair et al. (1997) though we have classified WD 0426+588 and WD 1544−377 as wide binaries (Tables 2 and 3) since the *Hipparcos* star is actually the companion. We include WD 2117+539 for which the *Hipparcos* parallax solution was rejected during the reduction process. WD 2007−303 and WD 2341+322 are *Hipparcos* degenerates not in Vauclair et al. (1997) while WD 0439+466, WD 0621−376, and WD 2211−495 are Tycho-2 white dwarfs. For HZ 43 (WD 1314+293), the *Hipparcos* parallax is known to be inconsistent with the predicted MRR (Vauclair et al. 1997), and we take instead the value from the Yale Parallax Catalog (van Altena et al. 1994). Only 6 of the *Hipparcos* white dwarfs and none of the Tycho-2 degenerates are present in *Gaia* DR1 owing to source filtering. The *Gaia* DR1 parallaxes and *G* magnitudes are identified in Table 1. In addition to the random errors available in the catalog, we have added a systematic error of 0.3 mas (Gaia Collaboration 2016).

Our limited search radius of 10″ around *Hipparcos* and Tycho-2 coordinates, which was designed to recover all white dwarfs that are directly in *Gaia* DR1, does not allow to build a meaningful sample of wide binaries. A list of white dwarfs that are in common proper motion pairs with *Hipparcos* or Tycho-2 stars was compiled from the literature (Silvestri et al. 2002; Gould & Chanamé 2004; Holberg et al. 2013; Zuckerman 2014). Our aim is not to have a complete sample but rather to include most known *Gaia* DR1 stars with wide degenerate companions. The 62 selected binary systems are identified in Table 2 along with their angular separation. Among those, 39 are primary stars with *Hipparcos* parallaxes collected in Table 3, and 23 are Tycho-2 stars with no prior distance measurements. We have found 46 of these primary stars in *Gaia* DR1, with parallaxes identified in Table 3. The resulting physical separations lead to orbital periods longer than those of Procyon and Sirius (> 40 yr), hence these orbital motions should have a minor impact on parallax determinations. We can derive the semi-empirical MRR for members of wide binaries in the same way as we do for directly observed white dwarfs. *Gaia* DR1 *G* magnitudes are available for 43 of the white dwarf companions, while *V* magnitudes can be found in the literature for most systems.

Our search has also recovered a large number of white dwarfs in unresolved binaries, often in Sirius-like systems where the degenerate star is only visible in the UV (Holberg et al. 2003). Whenever there was no optical spectroscopy for these objects, we have neglected them from our sample, since their atmospheric parameters are significantly less precise than for the white dwarfs identified in Tables 1 and 3. This includes WD 1736+133 and WD 1132−325, even though they are separated by more than 4″ from their bright companion (Holberg et al. 2013).

2.1 Spectroscopic Parameters

Precise atmospheric parameters determined from spectroscopic fits are a critical ingredient to extract the semi-empirical MRR. As a consequence, we have ensured that we have a homogeneous determination of the atmospheric parameters by using the same models and fitting technique for the whole sample as much as feasible. Whenever possible, atmospheric parameters for DA white dwarfs are taken from Gianninas et al. (2011), or in a few cases from Tremblay et al. (2011) and Limoges et al. (2015). These studies are based on the model spectra from Tremblay et al. (2011), and 3D corrections from Tremblay et al. (2013) were applied when appropriate. The uncertainties in Gianninas et al. (2011) are the sum of the formal χ^2 errors and external errors of 1.2% in $T_{\rm eff}$ and 0.038 dex in $\log g$. The latter were determined by observing selected stars on different nights and at different sites (Liebert et al. 2005). There are five DA white dwarfs, all in wide binaries, that are not part of the Gianninas et al. (2011) sample. For WD 0315−011, ϵ Ret B, WD 0842+490, WD 1209−060, and HS 2229+2335, we use the atmospheric parameters of Catalán et al. (2008), Farihi et al. (2011), Vennes et al. (1997), Kawka & Vennes (2010), and Koester et al. (2009), respectively. Except for Farihi et al. (2011), these studies were performed prior to the inclusion of the Tremblay & Bergeron (2009) Stark profiles, hence we have corrected for this effect using fig. 12 of Tremblay & Bergeron (2009) and added 3D corrections when appropriate. Finally, WD 0221+399, WD 0433+270, WD 751−252, WD 1750+098, and WD 2253+054 have very weak Balmer lines, hence they have no spectroscopic gravities.

A few hot white dwarfs that are identified with spectral type DA+BP (or DAO+BP) have the so-called Balmer line problem (Werner 1996). In those cases, the Gianninas et al. (2011) solution is with CNO added to the model atmospheres. We also note that the optical spectrum of HZ 43 employed by Gianninas et al. (2011) shows some evidence of contamination from the close M dwarf companion. As a consequence, the error bars for this star should be taken with some caution.

For the DB white dwarfs WD 0615−591, WD 0845−188, and WD 2129+004, we use the atmospheric parameters from

Table 1. Parallaxes of Directly Observed White Dwarfs

WD	Alt. Name	HIP/Tycho ID	π (Gaia) [mas]	G (Gaia) [mag]	π (other) [mas]	Ref	V [mag]	Ref	SpT	$T_{\rm eff}$ [K]	log(g) (spec) [cm^2/s]	Ref
0046+051	vMa 2	HIP 3829	...	...	234.60 (5.90)	1	12.37 (0.02)	4	DZ	6220 (180)	...	10
0148+467	GD 279	HIP 8709	...	...	64.53 (3.40)	1	12.44 (0.03)	4	DA	14,000 (280)	8.04 (0.04)	11
0227+050	Feige 22	HIP 11650	...	...	37.52 (5.17)	1	12.78 (0.01)	4	DA	19,920 (310)	7.93 (0.05)	11
0232+035	Feige 24	HIP 12031	13.06 (1.06)	12.177 (0.004)	10.90 (3.94)	1	12.41 (0.01)	4	DA+dM	66,950 (1440)	7.40 (0.07)	11
0310−688	LB 3303	HIP 14754	...	...	97.66 (1.85)	1	11.39 (0.01)	5	DA	16,860 (240)	8.09 (0.04)	11
0439+466	SH 2-216	TYC 3343-1571-1	...	...	7.76 (0.33)	2	12.62 (0.03)	6	DAO+BP	86,980 (2390)	7.23 (0.08)	11
0501+527	G 191-B2B	HIP 23692	...	...	16.70 (2.97)	1	11.78 (0.01)	4	DA	60,920 (990)	7.55 (0.05)	11
0621−376	TYC 7613-1087-1	TYC 7613-1087-1	...	...	...	...	12.09 (0.03)	6	DA+BP	66,060 (1140)	7.12 (0.05)	11
0644+375	He 3	HIP 32560	...	...	63.53 (3.55)	1	12.06 (0.01)	4	DA	22,290 (340)	8.10 (0.05)	11
1134+300	GD 140	HIP 56662	...	...	63.26 (3.60)	1	12.49 (0.02)	4	DA	22,470 (340)	8.56 (0.05)	11
1142−645	L 145-141	HIP 57367	215.78 (0.57)	11.410 (0.002)	215.80 (1.25)	1	11.51 (0.01)	5	DQ	7970 (220)	...	10
1314+293	HZ 43A	HIP 64766	17.23 (0.77)	12.907 (0.002)	15.50 (3.40)	2	12.91 (0.03)	4	DA+dM	56,800 (1250)	7.89 (0.07)	11
1327−083	Wolf 485A	HIP 65877	...	...	57.55 (3.85)	1	12.34 (0.01)	5	DA	14,570 (240)	7.99 (0.04)	11
1337+705	G 238-44	HIP 66578	...	...	38.29 (3.02)	1	12.77 (0.01)	7	DA	21,290 (330)	7.93 (0.05)	11
1620−391	CD −38 10980	HIP 80300	...	...	76.00 (2.56)	1	11.01 (0.01)	4	DA	25,980 (370)	7.96 (0.04)	11
1647+591	G 226-29	HIP 82257	91.04 (0.80)	12.288 (0.001)	94.04 (2.67)	1	12.24 (0.03)	4	DAV	12,510 (200)	8.34 (0.05)	11, 12
1917−077	LDS 678A	HIP 95071	95.10 (0.77)	12.248 (0.001)	91.31 (4.02)	1	12.29 (0.01)	5	DBQA	10,400 (360)	...	10
2007−303	L 565-18	HIP 99438	...	...	61.09 (4.51)	1	12.24 (0.01)	5	DA	16,150 (230)	7.98 (0.04)	11
2032+248	Wolf 1346	HIP 101516	...	...	64.32 (2.58)	1	11.55 (0.01)	5	DA	20,700 (320)	8.02 (0.05)	11
2039−202	L 711-10	HIP 102207	...	...	48.22 (3.77)	1	12.40 (0.01)	5	DA	20,160 (300)	7.98 (0.04)	11
2117+539	G 231-40	TYC 3953-480-1	57.76 (0.99)	12.411 (0.001)	50.70 (7.00)	3	12.33 (0.01)	4	DA	14,680 (240)	7.91 (0.05)	11
2149+021	G 93-48	HIP 107968	...	...	37.51 (4.41)	1	12.74 (0.01)	8	DA	18,170 (270)	8.01 (0.04)	11
2211−495	TYC 8441-1261-1	TYC 8441-1261-1	...	...	...	...	11.71 (0.01)	9	DA+BP	71,530 (1530)	7.46 (0.06)	11
2341+322	LP 347-4	HIP 117059	...	...	58.39 (11.79)	1	12.93 (0.05)	4	DA	13,100 (200)	8.02 (0.04)	11, 12

Notes. The *Gaia* uncertainties include both the random errors and a systematic error of 0.3 mas (Gaia Collaboration 2016). Only spectroscopic log g determinations are included and not the derivations based on the parallax measurements. DA+BP stands for a DA white dwarf with the Balmer line problem (see Section 2.1). **References.** 1) van Leeuwen (2007), 2) Harris et al. (2007), 3) van Altena et al. (1994), 4) Vauclair et al. (1997), 5) Koen et al. (2010), 6) McCook & Sion (1999), 7) Landolt & Uomoto (2007), 8) Landolt (2009), 9) Marsh et al. (1997), 10) Giammichele et al. (2012), 11) Gianninas et al. (2011), 12) Tremblay et al. (2013).

Bergeron et al. (2011). Even though they are in the regime $T_{\rm eff} < 16,000$ K, where spectroscopic log g determinations are unreliable (Bergeron et al. 2011; Koester & Kepler 2015), we keep them in the sample as Section 3 demonstrates that they are in agreement with the theoretical MRRs when parallaxes are available. However, we make no attempt to determine whether a thin H-layer is more appropriate for these objects, as suggested from the lack of hydrogen at the surface. On the other hand, WD 0551+123 and WD 1917−077 are too cool for a meaningful log g determination from the He I lines.

For 15 DC, 1 probable DB, 4 DQ, 4 DZ, and 2 probable white dwarfs, there are no spectroscopic log g determinations, hence no independent mass determinations apart from using the parallaxes and magnitudes from Tables 1 and 3, combined with a theoretical MRR. We do not perform such mass determinations as it is outside the scope of this work to review the photometric fits of these objects. We only include the 48 DA and 2 DB white dwarfs with spectroscopic log g values and at least one parallax measurement in our analysis.

3 THE MASS-RADIUS RELATION

We employ the method of Vauclair et al. (1997) to study the semi-empirical MRR. The first step is to define the surface flux in erg sec^{-1} cm^{-2} Å^{-1} from the predicted emergent monochromatic Eddington flux H_λ,

$$F_{\rm surface} = 4\pi H_\lambda(T_{\rm eff}, \log g) \, , \tag{1}$$

where we have explicitly included the dependence on the atmospheric parameters. The flux measured at the earth is

$$f_{\rm earth} = \frac{R^2}{D^2} F_{\rm surface} \, , \tag{2}$$

which fully accounts for limb-darkening. However, the flux is usually integrated over some characteristic photometric passband, such as Johnson-Kron-Cousins V or *Gaia* G, and measured by a photon-counting device. Conversely, a surface magnitude $m_{\rm o}$ can be predicted

$$m_{\rm o} = -2.5 \log \left(\frac{\int S(\lambda) F_{\rm surface} \lambda d\lambda}{\int S(\lambda) \lambda d\lambda} \right) + C_S \, , \tag{3}$$

where $S(\lambda)$ is the total system quantum efficiency and C_s is the zero point. The zero point for the V filter is defined from the Vega magnitude of +0.026 which results in $C_V = -21.0607$ (Holberg & Bergeron 2006). If we use the same procedure as Holberg & Bergeron (2006) for the *Gaia* G filter where Vega has a magnitude of +0.03 (Jordi et al. 2010), we obtain $C_G = -21.48050$. The radius is then found from

$$\log R/R_\odot = 0.2(m_{\rm o} - m) - \log \pi[{\rm arcsec}] + 7.64697 \, , \tag{4}$$

where π is the trigonometric parallax in arcsec, m is the apparent magnitude, and the constant is log(parsec/$R_\odot$).

A correction for interstellar extinction could be necessary for white dwarfs with parallaxes smaller than about 20 mas (Genest-Beaulieu & Bergeron 2014). For the magnitude-limited directly observed *Hipparcos* white dwarf sample, this corresponds to $T_{\rm eff} \gtrsim 50,000$ K, including G191−B2B which is suggested to have a small reddening of $E(B-V) = 0.0005$ (Bohlin et al. 2014). Nevertheless, it is difficult to calculate individual corrections that would be appropriate for our sample, and we neglect this effect.

The emergent fluxes from the model atmospheres of

Table 2. White Dwarfs in Wide Binaries: Binary Parameters

WD	Alt. Name	Primary	HIP/Tycho ID	V (primary) [mag]	Sep. [arcsec]	Ref
0030+444	G 172-4	BD +43 100	HIP 2600	10.28	28.8	1
0042+140	LP 466-033	BD +13 99	HIP 3550	9.79	62.4	1
0148+641	G 244-36	G 244-37	TYC 4040-1662-1	11.38	12.1	2
0220+222	G 94-B5B	HD 14784	TYC 1221-1534-1	8.24	26.9	3
0221+399	LP 196-060	BD +39 539	TYC 2835-349-1	9.84	40.5	1
0250−007	LP 591-177	HD 17998	TYC 4700-510-1	9.11	27.4	1
0304+154	LP 471-52	LP 471-51	TYC 1225-1388-1	11.49	20.6	1
0315−011	LP 592-80	BD −01 469	HIP 15383	5.37	46.1	1
0355+255	NLTT 12250	HD 283255	TYC 1817-1583-1	10.82	16.0	3
0400−346	NLTT 12412	HD 25535	HIP 18824	6.73	64.1	1
0413−077	40 Eri B	40 Eri A	HIP 19849	4.43	83.4	1
0415−594	ϵ Ret B	ϵ Ret	HIP 19921	4.44	12.9	1
0426+588	Stein 2051B	LHS 26	HIP 21088	10.98	8.9	1
0433+270	G 39-27	HD 283750	HIP 21482	8.42	124	1
0551+123	NLTT 15768	HD 39570	HIP 27878	7.76	89.8	1
0615−591	BPM 18164	HD 44120	HIP 29788	6.43	40.7	1
0642−166	Sirius B	Sirius A	HIP 32349	−1.46	8.1	1
0642−285	LP 895-41	CD −28 3358	TYC 6533-994-1	10.57	16.1	1
0658+712	LP 34-137	BD +71 380	HIP 34082	9.34	28.7	1
0736+053	Procyon B	Procyon	HIP 37279	0.37	4.8	1
0743−336	VB 03	HD 63077	HIP 37853	5.37	868	1
0751−252	SCR J0753-2524	NLTT 18618	HIP 38594	9.72	400	4
0842+490	HD 74389B	HD 74389	HIP 42994	7.48	20.1	1
0845−188	LP 786-6	NLTT 20261	TYC 6020-1448-1	11.23	30.2	1
1009−184	WT 1759	BD −17 3088	HIP 49973	9.91	399	1
1043−188	LP 791-55	BD −18 3019A	HIP 52621	11.21	7.1	2
1107−257	LP 849-059	HD 96941	HIP 54530	8.69	100.2	1
1120+073	LP 552-49	LP 552-48	HIP 55605	10.38	23.2	2
1130+189	LP 433-6	LP 433-7	TYC 1438-418-2	11.15	154.5	1
1133+619	LP 94-65	LP 94-66	TYC 4153-706-1	11.77	17.72	1
1209−060	LP 674-029	HD 106092	HIP 59519	10.14	203	1
1304+227	SDSS J1307+2227	BD +23 2539	TYC 1456-876-1	9.75	20.5	1
1354+340	G 165-B5B	BD +34 2473	HIP 68145	9.08	55.7	1
1455+300	NLTT 38926	BD +30 2592	HIP 73224	9.73	25.9	1
1501+301	LP 326-74	LP 326-75	TYC 2023-1076-1	12.14	88.4	1
1542+729	LP 42-164	LP 42-163	HIC 76902	10.85	18.4	1
1544−377	L 481-60	HD 140901	HIP 77358	6.01	14.8	1
1554+215	PG 1554+215	BD +21 2850	TYC 1502-1772-1	10.16	75.7	5
1619+123	PG 1619+123	HD 147528	HIP 80182	8.19	62.5	1
1623+022	NLTT 42785	BD +02 3101	HIP 80522	10.07	9.6	1
1623−540	L 266-196	L 266-195	TYC 8712-1589-1	11.92	39.7	2
1659−531	BPM 24602	BPM 24601	HIP 83431	5.29	113.5	1
1706+332	G 181-B5B	BD +33 2834	HIP 83899	8.59	37.6	1
1710+683	LP 70-172	LP 70-171	TYC 4421-2830-1	11.46	27.8	1
1743−132	G 154-B5B	G 154-B5A	HIP 86938	11.91	32.2	2
1750+098	G 140-B1B	HD 162867	TYC 1011-534-1	9.41	24.7	1
1848+688	NLTT 47097	BD +68 1027	HIP 92306	9.72	33.9	1
2048+809	LP 25-436	BD +80 670	TYC 4598-133-1	9.08	18.56	1
2054−050	NLTT 50189	Ross 193	HIP 103393	11.92	15.5	6
2129+000	LP 638−004	BD −00 4234	HIP 106335	9.89	133	1
2154−512	BPM 27606	CD −51 13128	HIP 108405	10.49	28.5	3
PM J21117+0120	...	...	TYC 527-72-1	10.65	33.5	5
2217+211	LP 460-003	BD +20 5125	HIP 110218	10.07	83.2	1
HS 2229+2335	...	HD 213545	TYC 2219-1647-1	8.40	110.10	5
SDSS J2245−1002	PB 7181	BD −10 5983	TYC 5815-1030-1	10.30	60.4	5
2253+054	NLTT 55300	GJ 4304	HIP 113244	11.21	17.1	2
2253+812	LP 002-697	G 242-15	TYC 4613-31-1	11.80	7.2	2
2253−081	BD −08 5980B	HD 216777	HIP 113231	8.01	41.8	1
2258+406	G 216-B14B	G 216-B14A	TYC 3220-1119-1	11.57	26.1	1
2301+762	LP 027-275	HD 218028	HIP 113786	8.75	13.4	1
2344−266	NLTT 57958	CD −27 16448	HIP 117308	11.46	13.2	2
2350−083	G 273-B1B	BD −08 6206	TYC 5831-189-1	11.00	23.7	1

References. 1) Holberg et al. (2013), 2) Silvestri et al. (2002), 3) Oswalt & Strunk (1994), 4) Zuckerman (2014), 5) this work, 6) Gould & Chanamé (2004).

Tremblay et al. (2011) were integrated over the *Gaia G* passband using Eq. 3 as was done in the preparatory work of Carrasco et al. (2014). The resulting radii $R_{\rm Gaia}$ from Eq. 4 are given in Table 4. The results using instead the *Hipparcos* or ground-based parallaxes ($R_{\rm Hipparcos}$) are also shown in Table 4. In those cases, we have still employed the apparent *Gaia G* magnitudes when available.

Traditionally, the next step has been to compute a mass independently of the MRR by combining the radii determined above with the spectroscopic $\log g$. These masses are given in Table 4 and presented in a M-R diagram in Fig. 2 for both the *Gaia* DR1 (top panel) and *Hipparcos* parallaxes (bottom panel). We note that the errors typically form elongated ellipses (Holberg et al. 2012) corresponding to the fact that M is a function of R^2. Furthermore, the predicted positions on the M-R diagram depend on $T_{\rm eff}$, as illus-

Table 3. Parallaxes of White Dwarfs in Wide Binaries

WD	Alt. Name	π (Gaia) [mas]	G (Gaia) [mag]	π (other) [mas]	Ref	V [mag]	Ref	SpT	$T_{\rm eff}$ [K]	log(g) (spec) [cm^2/s]	Ref
0030+444	G 172-4	13.97 (0.80)	16.550 (0.002)	11.22 (1.52)	1	16.44 (0.05)	2	DA	10,270 (150)	8.03 (0.05)	12, 13
0042+140	LP 466-033	17.41 (0.57)	18.405 (0.005)	14.38 (1.44)	1	18.79 (0.05)	3	DZA	5070 (90)	...	14
0148+641	G 244-36	57.63 (0.70)	13.938 (0.001)	...	...	14.00 (0.05)	2	DA	9000 (130)	8.14 (0.05)	12, 13
0220+222	G 94-B5B	12.74 (0.55)	...	...	...	15.83 (0.05)	2	DA	16,240 (280)	8.05 (0.05)	12
0221+399	LP 196-060	24.30 (0.55)	17.071 (0.002)	...	...	17.39 (0.05)	2	DA	6250 (140)	8.30 (0.23)	12, 13
0250−007	LP 591-177	21.00 (0.89)	16.291 (0.003)	...	...	16.40 (0.05)	2	DA	8410 (130)	8.20 (0.07)	12, 13
0304+154	LP 471-52	...	19.11 (0.01)	...	...	20.20 (0.10)	2	DC:	...	...	2
0315−011	LP 592-80	...	17.493 (0.003)	14.89 (0.84)	1	17.20 (0.10)	2	DA	7520 (260)	7.97 (0.45)	15, 16, 13
0355+255	NLTT 12250	14.75 (0.57)	18.237 (0.004)	...	...	16.80 (0.10)	2	DC:	...	...	2
0400−346	NLTT 12412	...	17.417 (0.002)	19.35 (0.63)	1	17.82 (0.05)	4	DC	5100 (100)	...	4
0413−077	40 Eri B	...	...	200.62 (0.23)	1	9.520 (0.05)	2	DA	17,100 (260)	7.95 (0.04)	12
0415−594	ϵ Ret B	...	...	54.83 (0.15)	1	12.50 (0.05)	2	DA	15,310 (350)	7.88 (0.08)	17
0426+588	Stein 2051B	181.50 (0.92)	...	181.36 (3.67)	1	12.44 (0.05)	2	DC	7180 (180)	...	7
0433+270	G 39-27	57.22 (0.58)	15.531 (0.001)	55.66 (1.43)	1	15.79 (0.06)	5	DA	5630 (100)	...	7
0551+123	NLTT 15768	...	15.758 (0.002)	8.68 (0.81)	1	15.87 (0.05)	4	DB	13,200 (900)	...	4
0615−591	BPM 18164	...	...	26.72 (0.29)	1	14.09 (0.10)	2	DB	15,750 (370)	8.04 (0.07)	18
0642−166	Sirius B	...	...	380.11 (1.26)	1	8.440 (0.06)	6	DA	25,970 (380)	8.57 (0.04)	12
0642−285	LP 895-41	15.34 (0.54)	16.422 (0.002)	...	...	16.60 (0.05)	2	DA	9280 (130)	7.87 (0.05)	12, 13
0658+712	LP 34-137	13.04 (0.68)	18.627 (0.004)	12.27 (1.37)	1	19.20 (0.10)	2	DC	...	...	2
0736+053	Procyon B	...	...	284.56 (1.26)	1	10.94 (0.05)	7	DQZ	7870 (430)	...	7
0743−336	VB 03	...	...	65.75 (0.51)	1	16.59 (0.05)	4	DC	4460 (100)	...	7
0751−252	SCR0753-2524	56.23 (0.56)	15.99 (0.07)	51.52 (1.46)	1	16.27 (0.05)	7	DA	5090 (140)	...	7
0842+490	HD 74389B	...	...	8.97 (0.57)	1	15.00 (0.05)	2	DA	40,250 (300)	8.09 (0.05)	19, 16
0845−188	LP 786-6	...	15.648 (0.002)	...	...	15.68 (0.03)	8	DB	17,470 (420)	8.15 (0.08)	18
1009−184	WT 1759	...	15.280 (0.002)	58.20 (1.67)	1	15.44 (0.05)	7	DZ	6040 (360)	...	7
1043−188	LP 791-55	52.59 (0.69)	...	49.95 (2.26)	...	15.52 (0.05)	7	DQpec	5780 (90)	...	7
1107−257	LP 849-059	24.18 (0.55)	17.273 (0.002)	24.90 (0.98)	1	16.79 (0.05)	2	DC	...	...	2
1120+073	LP 552-49	...	17.159 (0.003)	31.12 (2.35)	1	17.49 (0.05)	2	DC	4460 (110)	...	20
1130+189	LP 433-6	4.63 (0.73)	17.569 (0.003)	...	...	17.60 (0.10)	2	DA	10,950 (190)	8.34 (0.06)	12, 13
1133+619	LP 94-65	7.05 (0.80)	18.358 (0.002)	...	...	17.70 (0.10)	2	DZ	...	...	2
1209−060	LP 674-029	22.69 (0.79)	16.878 (0.004)	22.18 (1.49)	1	17.26 (0.05)	2	DA	6590 (100)	8.02 (0.22)	4
1304+227	SDSS J1307+2227	12.96 (0.58)	16.491 (0.002)	...	...	16.20 (0.10)	2	DA	10,280 (180)	8.21 (0.09)	12, 13
1354+340	G 165-B5B	10.79 (0.58)	16.023 (0.004)	10.06 (1.15)	1	16.17 (0.01)	5	DA	14,490 (290)	8.06 (0.05)	12
1455+300	NLTT 38926	15.48 (0.55)	18.418 (0.004)	16.51 (1.66)	1	20.16 (0.10)	9	...	...	...	9
1501+301	LP 326-74	12.56 (1.06)	17.654 (0.001)	...	...	17.70 (0.10)	2	DC	7250	...	21
1542+729	LP 42-164	13.44 (0.52)	18.077 (0.004)	16.10 (2.48)	1	18.06 (0.05)	10	DC	...	...	10
1544−377	L 481-60	65.57 (0.74)	13.003 (0.001)	65.13 (0.40)	1	12.80 (0.05)	2	DA	10,380 (150)	7.96 (0.04)	12, 13
1554+215	PG 1554+215	9.73 (0.68)	...	...	...	15.26 (0.01)	5	DA	27,320 (410)	7.90 (0.05)	12
1619+123	PG 1619+123	17.70 (0.53)	...	19.29 (1.02)	1	14.66 (0.05)	2	DA	17,150 (260)	7.87 (0.04)	12
1623+022	NLTT 42785	20.59 (0.61)	17.50 (0.01)	17.64 (2.12)	1	17.42 (0.05)	9	DC	...	...	10
1623−540	L 266-196	21.82 (0.66)	15.445 (0.002)	...	...	15.74 (0.05)	2	DA	11,280 (170)	7.95 (0.04)	12, 13
1659−531	BPM 24602	...	...	36.73 (0.63)	1	13.47 (0.05)	2	DA	15,570 (230)	8.07 (0.04)	12
1706+332	G 181-B5B	13.98 (0.53)	15.970 (0.002)	14.35 (0.87)	1	15.90 (0.05)	2	DA	13,560 (390)	7.94 (0.06)	12, 13
1710+683	LP 70-172	17.98 (0.75)	17.259 (0.007)	...	...	17.50 (0.05)	2	DA	6630 (230)	7.86 (0.51)	12, 13
1743−132	G 154-B5B	25.97 (0.75)	14.604 (0.002)	29.96 (3.63)	1	14.22 (0.05)	2	DA	12,920 (210)	8.01 (0.05)	12, 13
1750+098	G 140-B1B	22.80 (0.53)	15.615 (0.002)	...	...	15.72 (0.05)	2	DA	9520	...	12
1848+688	NLTT 47097	11.09 (0.52)	17.342 (0.004)	12.68 (0.76)	1	17.18 (0.05)	9	...	...	...	9
2048+809	LP 25-436	11.67 (1.02)	16.434 (0.002)	...	...	16.59 (0.05)	2	DA	8450 (130)	8.11 (0.07)	12, 13
2054−050	NLTT 50189	62.15 (0.73)	...	56.54 (3.92)	1	16.69 (0.05)	7	DC	4340 (80)	...	7
2129+000	LP 638-004	23.16 (0.52)	...	22.13 (2.01)	1	14.67 (0.03)	8	DB	14,380 (350)	8.26 (0.14)	18
2154−512	BPM 27606	66.13 (0.75)	14.477 (0.001)	62.61 (2.92)	1	14.74 (0.03)	7	DQP	7190 (90)	...	7
PM J21117+0120	...	16.37 (1.00)	15.266 (0.002)	...	...	...	...	DA	16,570 (100)	8.06 (0.05)	20
2217+211	LP 460-003	18.76 (0.60)	17.672 (0.004)	20.30 (1.40)	1	17.69 (0.05)	2	DC	...	...	22
HS 2229+2335	...	9.02 (0.85)	15.992 (0.004)	...	...	16.01 (0.09)	5	DA	20,000 (500)	7.96 (0.09)	23, 16
SDSS J2245−1002	PB 7181	16.72 (1.29)	...	...	...	17.02 (0.05)	11	DA	8700 (30)	8.36 (0.04)	11, 13
2253+054	NLTT 55300	40.06 (1.09)	...	40.89 (2.12)	1	15.71 (0.05)	2	DA	6240 (150)	8.60 (0.24)	12, 13
2253+812	LP 002-697	...	17.543 (0.003)	...	...	17.30 (0.10)	2	DC:	...	...	2
2253−081	BD −08 5980B	27.97 (0.54)	16.311 (0.002)	27.22 (1.12)	1	16.50 (0.05)	2	DA	6770 (130)	7.82 (0.18)	12, 13
2258+406	G 216-B14B	13.96 (0.73)	16.676 (0.002)	...	...	15.50 (0.10)	2	DA	9910 (150)	8.16 (0.06)	12, 13
2301+762	LP 027-275	15.60 (0.56)	...	14.97 (0.79)	1	16.35 (0.05)	2	DC	...	...	24
2344−266	NLTT 57958	21.50 (0.55)	16.673 (0.008)	20.03 (3.04)	1	16.59 (0.05)	2	DB:	...	...	2
2350−083	G 273-B1B	9.96 (1.13)	...	...	...	16.18 (0.10)	2	DA	19,270 (310)	7.90 (0.05)	12

Notes. The *Gaia* uncertainties include both the random errors and a systematic error of 0.3 mas (Gaia Collaboration 2016). Only spectroscopic log g determinations are included and not the derivations based on the parallax measurements. Spectral types with the ":" symbol are uncertain. **References.** 1) van Leeuwen (2007), 2) McCook & Sion (1999), 3) Kilic et al. (2010), 4) Kawka & Vennes (2010), 5) Zacharias et al. (2012), 6) Holberg et al. (1984), 7) Giammichele et al. (2012), 8) Landolt & Uomoto (2007), 9) Gould & Chanamé (2004), 10) Holberg et al. (2013), 11) Tremblay et al. (2011), 12) Gianninas et al. (2011), 13) Tremblay et al. (2013), 14) Kilic et al. (2010), 15) Catalán et al. (2008), 16) Tremblay & Bergeron (2009), 17) Farihi et al. (2011), 18) Bergeron et al. (2011), 19) Vennes et al. (1997), 20) Limoges et al. (2015), 21) Girven et al. (2011), 22) Hintzen (1986), 23) Koester et al. (2009), 24) Greenstein (1984).

trated in Fig. 2 by the theoretical MRRs from Wood (1995) and Fontaine et al. (2001) with thick H-layers at 10,000, 30,000, and 60,000 K. For these reasons, it is not straightforward to interpret the results in a M-R diagram. In particular, the data points in Fig. 2, both for the *Gaia* DR1 and *Hipparcos* samples, do not form a clear sequence of decreasing radius as a function of increasing mass as in the predicted MRR. This is in part caused by observational uncertainties, the fact that most white dwarfs in the sample have similar masses around ~0.6 $M_{\odot}$, and that for a given mass the radius will change as a function of $T_{\rm eff}$.

WD 1130+189 and WD 2048+809 are two peculiar white dwarfs in *Gaia* DR1 for which the observed radii $R_{\rm Gaia}$ are about twice the predicted values. Given the surface gravities, this would lead to spurious observed masses well above the Chandrasekhar mass limit. The natural explanation for this behaviour is that these wide binaries are actually rare triple systems with unresolved double degenerates (O'Brien et al. 2001; Andrews et al. 2016; Maxted et al. 2000). These white dwarfs had no parallax measurements until now and were not known to be double degenerates. However, high-resolution observations of WD 2048+809 show peculiar line cores that can not be explained by rotation or magnetic fields (Karl et al. 2005). Liebert et al. (1991) and Tremblay et al. (2011) have shown that double DA white dwarfs can almost perfectly mimic a single DA in spectroscopic and photometric analyses. As a consequence, it may not be surprising that *Gaia* is able to reveal for the first time the double degenerate nature of these objects.

In the following, we compare the *observed* radius $R_{\rm Gaia}$ or $R_{\rm Hipparcos}$ defined by Eq. 4 to a *predicted* radius $R_{\rm MRR}$ drawn from theoretical MRRs and spectroscopic atmospheric parameters, an approach also favoured by Holberg et al. (2012). We note that neither quantity is purely observed or purely predicted and both depend on the spectroscopic atmospheric parameters, hence model atmospheres. Nevertheless, $R_{\rm Gaia}$ depends almost only on $T_{\rm eff}$ while $R_{\rm MRR}$ depends largely on $\log g$. Theoretical MRRs with thick H-layers ($q_{\rm H} = 10^{-4}$) were employed for our standard derivation. For $M > 0.45\ M_{\odot}$, we use the evolutionary sequences of Fontaine et al. (2001, $T_{\rm eff} \leq 30{,}000$ K, C/O-core 50/50 by mass fraction mixed uniformly) and Wood (1995, $T_{\rm eff} > 30{,}000$ K, pure C-core). For lower masses we use the He-core sequences of Althaus et al. (2001).

Fig. 3 compares $R_{\rm Gaia}$ (top panel) and $R_{\rm Hipparcos}$ (bottom panel) to $R_{\rm MRR}$. The dotted black line centered on zero illustrates a perfect match between observations and theory for thick H-layers, while the dashed red line shows the match to an illustrative theoretical MRR with thin H-layers ($q_{\rm H} = 10^{-10}$) at 0.6 $M_{\odot}$. On average, the data agree with the theoretical MRR for thick H-layers within 0.99σ and 0.98σ for *Gaia* DR1 and *Hipparcos*, respectively, and no significant systematic offset is observed (neglecting the suspected double degenerates). The observed uncertainties for both samples do not allow, however, for meaningful constraints on H envelope masses. The error bars are only slightly smaller for the *Gaia* DR1 sample compared to *Hipparcos*. There are two reasons for this behaviour. First of all, most of the *Gaia* DR1 white dwarfs are companions to fairly distant but bright primary stars with parallaxes. While the absolute parallax error is on average 3 times smaller in *Gaia* DR1, the relative errors (σ_{π}/π) are comparable with 5.05% in *Gaia* DR1 and 7.06% for pre-*Gaia* measurements. Furthermore, the uncertainties from the atmospheric parameters become the dominant contribution for the *Gaia* DR1 sample (see Section 4.2). The implications of these results are further discussed in Section 4.

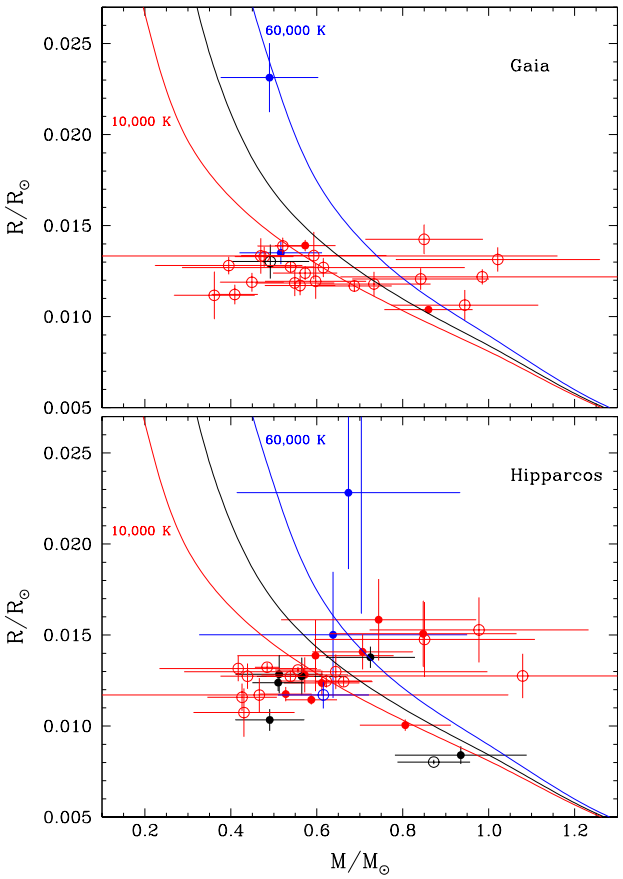

Figure 2. *(Top:)* semi-empirical MRR using *Gaia* DR1 and atmospheric parameters defined in Table 1 for directly observed white dwarfs (solid circles) and in Table 3 for wide binaries (open circles). Numerical values are given in Table 4. Theoretical MRRs for $q_{\rm H} = 10^{-4}$ (Wood 1995; Fontaine et al. 2001) at 10,000 K (red), 30,000 K (black), and 60,000 K (blue) are also shown. The data points are also colour coded based on their $T_{\rm eff}$ and the closest corresponding theoretical sequence. *(Bottom:)* Similar to the top panel but with pre-*Gaia* parallax measurements (mostly from *Hipparcos*) identified in Tables 1 and 3. We still rely on *Gaia G* magnitudes when available.

4 DISCUSSION

4.1 Comparison with Other Empirical Mass-Radius Relations

Our results can be compared to two empirical MRRs not drawn from *Gaia* DR1. Fig. 4 (top panel) shows an independent analysis for eclipsing and/or tidally distorted extremely low-mass (ELM) He-core white dwarf systems that provide model-independent radii (Hermes et al. 2014; Gianninas et al. 2014). The data are reproduced from table 7 of Tremblay et al. (2015) where 3D model atmosphere corrections were applied. The theoretical radius $R_{\rm MRR}$ is taken from the spectroscopic atmospheric parameters and the He-core MRR, similarly to our main analysis. The agreement with the theoretical He-core MRR for thick H-layers is on average within error bars. This result suggests that the consistency between the theoretical MRR and spectroscopic atmospheric parameters holds in the ELM regime as well.

Fig. 4 (bottom panel) also shows the results for eclipsing binaries where masses and radii are both directly constrained from the eclipses and orbital parameters. The selected systems from the lit-

Table 4. Semi-Empirical White Dwarf Mass-Radius Relation

WD	$M_{\rm Hipparcos}$ [$M_\odot$]	$R_{\rm Hipparcos}$ [$0.01R_\odot$]	$M_{\rm Gaia}$ [$M_\odot$]	$R_{\rm Gaia}$ [$0.01R_\odot$]	$R_{\rm MRR}$ [$0.01R_\odot$]
Directly Observed White Dwarfs					
0148+467	0.612 (0.088)	1.237 (0.068)	...	...	1.259 (0.034)
0227+050	0.597 (0.182)	1.387 (0.196)	...	...	1.372 (0.048)
0232+035	0.703 (0.596)	2.771 (1.153)	0.490 (0.113)	2.313 (0.190)	2.384 (0.151)
0310−688	0.587 (0.060)	1.144 (0.025)	...	...	1.221 (0.034)
0439+466	0.506 (0.104)	2.858 (0.126)	...	...	2.960 (0.226)
0501+527	0.674 (0.260)	2.282 (0.419)	...	...	2.049 (0.091)
0644+375	0.490 (0.080)	1.034 (0.059)	...	...	1.222 (0.044)
1134+300	0.935 (0.153)	0.840 (0.049)	...	...	0.857 (0.036)
1314+293	0.638 (0.312)	1.501 (0.346)	0.516 (0.096)	1.351 (0.062)	1.522 (0.087)
1327−083	0.706 (0.117)	1.408 (0.096)	...	...	1.304 (0.035)
1337+705	0.512 (0.101)	1.285 (0.103)	...	...	1.376 (0.048)
1620−391	0.510 (0.060)	1.239 (0.045)	...	...	1.360 (0.039)
1647+591	0.806 (0.106)	1.005 (0.031)	0.860 (0.103)	1.038 (0.016)	1.013 (0.038)
2007−303	0.572 (0.101)	1.282 (0.096)	...	...	1.316 (0.036)
2032+248	0.725 (0.104)	1.378 (0.059)	...	...	1.291 (0.046)
2039−202	0.565 (0.104)	1.274 (0.102)	...	...	1.326 (0.037)
2117+539	0.744 (0.227)	1.584 (0.224)	0.573 (0.071)	1.391 (0.030)	1.376 (0.046)
2149+021	0.847 (0.218)	1.507 (0.181)	...	...	1.294 (0.036)
2341+322	0.528 (0.060)	1.176 (0.039)	...	...	1.274 (0.035)
White Dwarfs in Wide Binaries					
0030+444	0.851 (0.257)	1.476 (0.206)	0.549 (0.092)	1.185 (0.072)	1.258 (0.042)
0148+641	...	...	0.687 (0.087)	1.169 (0.030)	1.165 (0.040)
0220+222	...	...	0.561 (0.082)	1.171 (0.053)	1.255 (0.044)
0250−007	...	...	0.842 (0.159)	1.207 (0.059)	1.116 (0.055)
0315−011	0.466 (0.579)	1.171 (0.093)	...	...	1.300 (0.382)
0413−077	0.556 (0.053)	1.308 (0.016)	...	...	1.346 (0.037)
0415−594	0.484 (0.028)	1.323 (0.024)	...	...	1.406 (0.019)
0615−591	0.622 (0.106)	1.247 (0.035)	...	...	1.263 (0.061)
0642−166	0.872 (0.084)	0.802 (0.012)	...	...	0.851 (0.029)
0642−285	...	...	0.478 (0.068)	1.329 (0.055)	1.392 (0.044)
0842+490	0.615 (0.106)	1.171 (0.075)	...	...	1.266 (0.049)
1130+189	...	...	...	2.061 (0.336)	1.012 (0.046)
1209−060	0.644 (0.353)	1.299 (0.094)	0.615 (0.329)	1.270 (0.051)	1.256 (0.180)
1304+227	...	...	1.021 (0.237)	1.314 (0.067)	1.111 (0.071)
1354+340	0.978 (0.255)	1.528 (0.179)	0.850 (0.137)	1.425 (0.080)	1.243 (0.043)
1544−377	0.539 (0.055)	1.273 (0.029)	0.539 (0.055)	1.273 (0.029)	1.318 (0.035)
1554+215	...	...	0.492 (0.090)	1.303 (0.093)	1.424 (0.052)
1619+123	0.439 (0.063)	1.274 (0.069)	0.521 (0.059)	1.388 (0.045)	1.421 (0.039)
1623−540	...	...	0.409 (0.054)	1.122 (0.053)	1.330 (0.035)
1659−531	0.663 (0.067)	1.244 (0.026)	...	...	1.236 (0.034)
1706+332	0.426 (0.081)	1.158 (0.075)	0.449 (0.074)	1.189 (0.052)	1.345 (0.054)
1710+683	...	...	0.470 (0.691)	1.333 (0.097)	1.390 (0.449)
1743−132	0.430 (0.117)	1.074 (0.133)	0.573 (0.075)	1.239 (0.038)	1.282 (0.043)
2048+809	...	...	...	2.018 (0.184)	1.188 (0.057)
PM J21117+0120	...	...	0.597 (0.118)	1.194 (0.096)	1.247 (0.044)
2129+000	1.079 (0.409)	1.275 (0.121)	0.985 (0.330)	1.219 (0.042)	1.078 (0.111)
HS 2229+2335	...	...	0.593 (0.169)	1.336 (0.130)	1.344 (0.085)
SDSS J2245−1002	...	...	0.944 (0.171)	1.063 (0.083)	0.994 (0.030)
2253−081	0.417 (0.183)	1.316 (0.069)	0.395 (0.171)	1.281 (0.049)	1.425 (0.158)
2258+406	...	...	0.733 (0.132)	1.179 (0.067)	1.151 (0.048)
2350−083	...	...	0.361 (0.093)	1.117 (0.129)	1.399 (0.048)

erature and their parameters are identified in Table 5. In those cases, the theoretical radius $R_{\rm MRR}$ is simply the dynamical mass processed through the theoretical MRR for thick H-layers, hence the prediction is independent of the atmospheric parameters. The error bars are significantly smaller than those shown in Fig. 3 for *Gaia* DR1 and *Hipparcos*, leading to a reduced y-axis scale in Fig. 4. As discussed in Parsons et al. (2016), in most cases the observed radius is in agreement with the theoretical MRR for thick H-layers. A mixture of He-cores ($M \leq 0.45\ M_\odot$) and C/O-cores were employed given the masses of the white dwarfs identified in Table 5. SDSS 0857+0342 with 0.514 $M_\odot$ is the one object in Fig. 4 that does not agree well with the C/O-core MRR. Parsons et al. (2012a) have suggested that it might instead be a He-core white dwarf.

It may not be entirely surprising that none of these post-common envelope systems are DB white dwarfs owing to the stellar wind of the companion. Very few hydrogen deficient degenerates are known in post-common envelope systems (see, e.g., Nagel et al. 2006). However, there is no evidence that the H envelope masses are necessarily close to the maximum value of $q_{\rm H} \sim 10^{-4}$, and the scatter observed in Fig. 4 could be due to these variations. We remind the reader that H envelope mass determinations are model dependent even for eclipsing binaries. The *Gaia* empirical MRR for single DA and DB white dwarfs could have more objects with

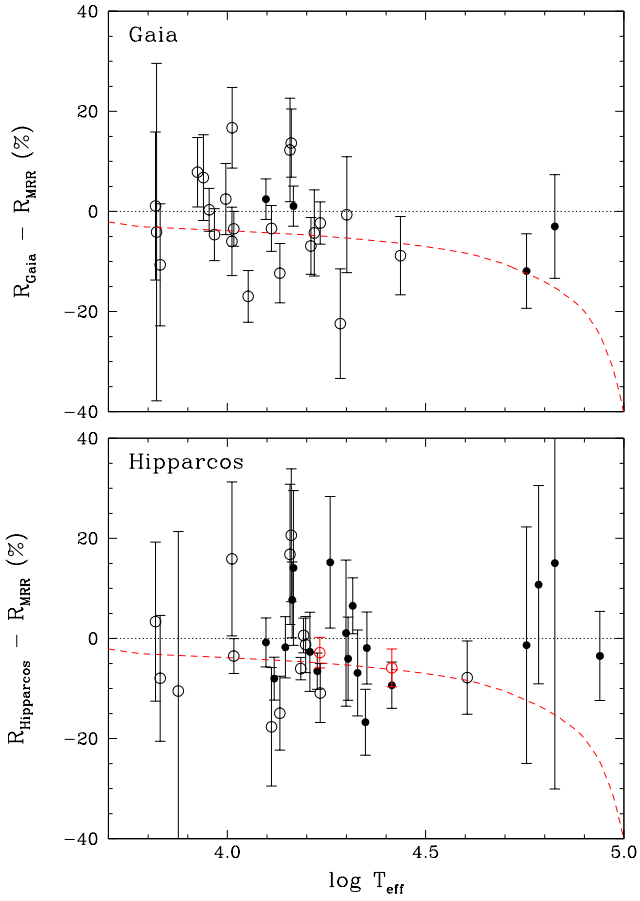

Figure 3. *(Top:)* Differences (in %) between observed *Gaia* DR1 radii $R_{\rm Gaia}$ (Eq. 4) and predicted radii $R_{\rm MRR}$ drawn from the MRR with thick H-layers ($q_{\rm H} = 10^{-4}$) as a function of $\log T_{\rm eff}$. Error bars for $\log T_{\rm eff}$ are omitted for clarity. Directly observed white dwarfs from Table 1 are represented by solid circles while wide binaries from Table 3 are illustrated by open circles. Numerical values are identified in Table 4. The dotted line $\Delta R = 0$ is shown as a reference and the dashed red line is for a MRR relation with thin H-layers ($q_{\rm H} = 10^{-10}$) at 0.6 $M_{\odot}$. *(Bottom:)* Similar to the top panel but with pre-*Gaia* parallax measurements (mostly from *Hipparcos*) identified in Tables 1 and 3. We still rely on *Gaia G* magnitudes when available. The benchmark cases 40 Eri B (cooler) and Sirius B (warmer) are shown in red.

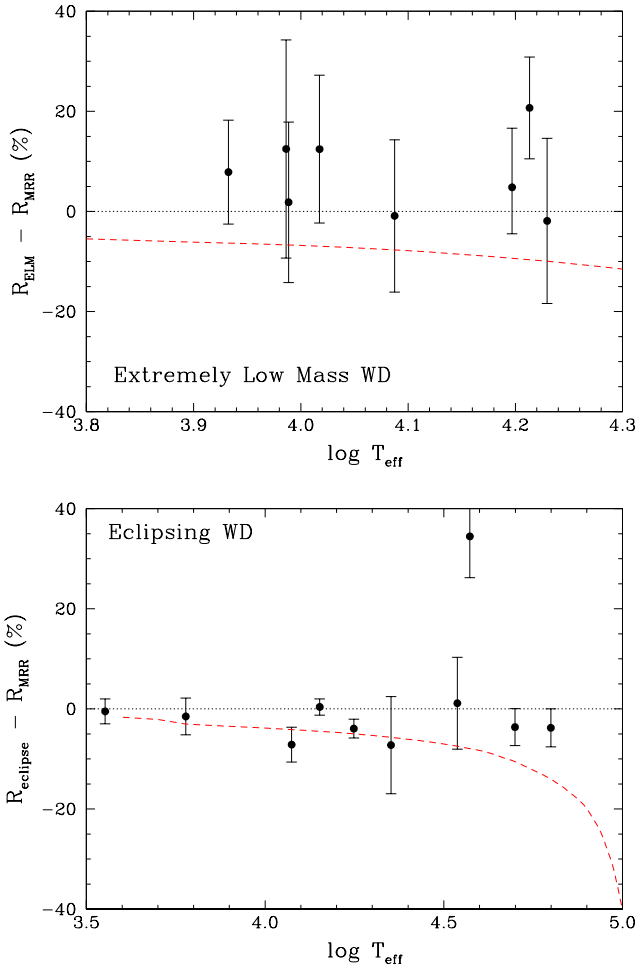

Figure 4. *(Top:)* Differences (in %) between observed radii $R_{\rm ELM}$ and predicted He-core radii $R_{\rm MRR}$ as a function of $\log T_{\rm eff}$ for the sample of He-core ELM white dwarfs from Gianninas et al. (2014) with 3D corrections from Tremblay et al. (2015). Error bars for $\log T_{\rm eff}$ are omitted for clarity and numerical values are presented in Tremblay et al. (2015). The dotted line $\Delta R = 0$ is shown as a reference and the dashed red line is for a He-core MRR relation with thin H-layers at 0.3 $M_{\odot}$. *(Bottom:)* Differences between observed radii $R_{\rm eclipse}$ and predicted radii $R_{\rm MRR}$ for eclipsing binaries for which there is an independent derivation of both the mass and radius. The observed sample of both He- and C/O-core white dwarfs drawn from the literature is described in Table 5. The dashed red line is for a MRR relation with thin H-layers at 0.6 $M_{\odot}$.

very thin H-layers, but there is no clear indication that the relation would be significantly different. In particular, the results of Fig. 4 for eclipsing binaries strongly suggest that theoretical MRRs are in agreement with observations. The semi-empirical MRR for the *Gaia* DR1 sample in Fig. 3 supports this conclusion, but it also indicates that the spectroscopic atmospheric parameters are on average consistent with *Gaia* DR1 parallaxes. In future *Gaia* data releases, the results from eclipsing binaries may provide the key to disentangle a genuine observed signature of the white dwarf MRR from a systematic effect from model atmospheres.

Finally, we note that Bergeron et al. (2007) compared gravitational redshift measurements with spectroscopically determined $\log g$ and a theoretical MRR, but the comparison remained inconclusive because of the large uncertainties associated with the redshift velocities.

4.2 Precision of the Atmospheric Parameters

The studies of Vauclair et al. (1997) and Provencal et al. (1998) have pioneered the derivation of the semi-empirical MRR for white dwarfs using precise *Hipparcos* parallaxes. Our work with *Gaia* DR1 parallaxes is in continuation of this goal. We remind the reader that such observed MRR is still highly dependent on the white dwarf atmospheric parameters, hence model atmospheres. In previous studies, parallax errors were often dominant, but with *Gaia* DR1 parallaxes, errors on spectroscopic atmospheric parameters are becoming the most important. Fig. 5 illustrates the error budget on $R_{\rm Gaia} - R_{\rm MRR}$ derived in Fig. 3 and demonstrates that the uncertainties on $T_{\rm eff}$ and $\log g$ marginally dominate. The number and precision of parallaxes will increase significantly with future *Gaia* data releases. In particular, the individual parallaxes in DR2 will

Table 5. Empirical Mass-Radius Relation from Eclipsing Binaries

Name	$M_{\rm eclipse}$ [$M_\odot$]	$R_{\rm eclipse}$ [$0.01R_\odot$]	$R_{\rm MRR}$ [$0.01R_\odot$]	$T_{\rm eff}$ [K]	Ref
NN Ser	0.535 (0.012)	2.08 (0.02)	2.16 (0.08)	63000 (3000)	1
V471 Tau	0.840 (0.050)	1.07 (0.07)	1.06 (0.07)	34500 (1000)	2
SDSS J1210+3347	0.415 (0.010)	1.59 (0.05)	1.61 (0.03)	6000 (200)	3
SDSS J1212−0123	0.439 (0.002)	1.68 (0.03)	1.75 (0.01)	17710 (40)	4
GK Vir	0.562 (0.014)	1.70 (0.03)	1.76 (0.06)	50000 (670)	4
SDSS 0138−0016	0.529 (0.010)	1.31 (0.03)	1.32 (0.01)	3570 (100)	5
SDSS 0857+0342	0.514 (0.049)	2.47 (0.08)	1.74 (0.15)	37400 (400)	6
CSS 41177A	0.378 (0.023)	2.224 (0.041)	2.39 (0.22)	22500 (60)	7
CSS 41177B	0.316 (0.011)	2.066 (0.042)	2.21 (0.06)	11860 (280)	7
QS Vir	0.781 (0.013)	1.068 (0.007)	1.064 (0.016)	14220 (350)	8

References. 1) Parsons et al. (2010), 2) O'Brien et al. (2001), 3) Pyrzas et al. (2012), 4) Parsons et al. (2012b), 5) Parsons et al. (2012c), 6) Parsons et al. (2012a), 7) Bours et al. (2015), 8) Parsons et al. (2016).

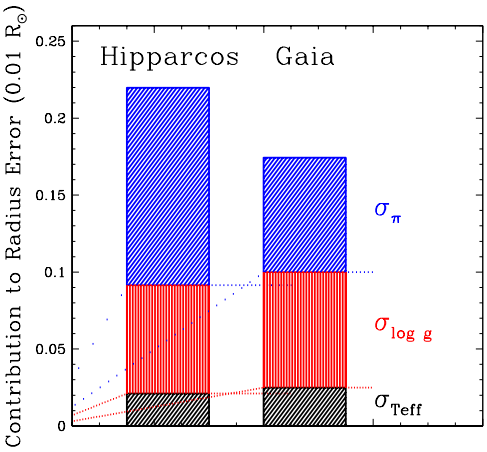

Figure 5. Average error budget in the comparison of observed radii ($R_{\rm Gaia}$ or $R_{\rm Hipparcos}$) and predicted radii ($R_{\rm MRR}$) in Fig. 3. The different uncertainties are identified in the legend.

have significantly higher individual precision due to a longer measurement time (22 months instead of 11 months, which is already 36% of the total mission time). Systematic errors are also expected to decrease significantly resulting from a more sophisticated calibration, including a better definition of the line spread function, the application of a chromaticity correction, a more accurate calibration of the basic angle variation, and a calibration and correction of micro clanks. On the other hand, it is not expected that the precision on the atmospheric parameters will markedly improve anytime soon.

We propose that the bright and well-studied single DA white dwarfs in the *Hipparcos* sample, unfortunately largely missing from *Gaia* DR1, may be used as a benchmark to understand the precision of the semi-empirical MRR of future *Gaia* data releases. We will now assess the possibility of improving the precision on the atmospheric parameters for these white dwarfs, taking WD 1327−083 as an example. There are three steps in the Balmer line fitting procedure that could introduce errors; uncertainties in the spectroscopic data, issues with the fitting procedure, and inaccuracies in the model atmospheres. To illustrate this, we have derived the atmospheric parameters of WD 1327−083 using a number of observations and methods. In Fig. 6 we display the published Gianninas et al. (2011) atmospheric parameters based on one spectrum. The formal χ^2 uncertainty is represented by the smaller dash-dotted ellipse. We remind the reader that the error bars from Gianninas et al. (2011) combine in quadrature this formal χ^2 error and a fixed external error of 1.2% in $T_{\rm eff}$ and 0.038 dex in $\log g$, resulting in the corresponding 1σ and 2σ error ellipses shown in Fig. 6.

First of all, we rely on 12 alternative spectra for WD 1327−083. These are all high signal-to-noise (S/N > 50) observations that were fitted with the same model atmospheres (Tremblay et al. 2011) and the same fitting code as in Gianninas et al. (2011). In all cases the formal χ^2 error is very similar to the one illustrated in Fig. 6 for the spectrum selected in Gianninas et al. (2011). We employ 7 spectra taken by the Montreal group from different sites (black filled points in Fig. 6) in addition to the one selected in Gianninas et al. (2011). We also rely on 3 UVES/VLT spectra taken as part of the SPY survey (Koester et al. 2009), shown with cyan filled circles in Fig. 6. Additionally, new observations were secured. The first one is a high S/N X-SHOOTER/VLT spectrum taken on programme 097.D-0424(A). The Balmer lines suggest a significantly warmer temperature (blue filled circle) than the average in Fig. 6. However, the calibrated spectra show a smaller than predicted flux in the blue, suggesting the offset could be caused by slit losses during the observations. Finally, we have recently obtained STIS spectrophotometry for WD 1327−083 under *Hubble Space Telescope* program 14213 as shown in Fig. 7. The Balmer lines were fitted and a solution (red filled circle in Fig. 6) very similar to that of Gianninas et al. (2011) was obtained.

The atmospheric parameters in Fig. 6, determined from different spectroscopic data, show a relatively large scatter that is significantly higher than the χ^2 error, confirming that external errors from the data reduction must be accounted for. The scatter appears slightly larger than the systematic uncertainty estimated by Liebert et al. (2005) and Gianninas et al. (2011) from a similar procedure. However, one could argue that some of the observations selected in this work should have a lower weight in the average since they show minor deficiencies in their instrumental setup or flux calibration.

The STIS spectrophotometry, which is calibrated using the three hot ($T_{\rm eff} > 30,000$ K) white dwarfs GD 71, GD 153, and G191−B2B (Bohlin et al. 2014), also permits the determination of the atmospheric parameters based on the continuum flux. The surface gravity was fixed at $\log g = 8.0$ since the sensitivity of the continuum flux to this parameter is much smaller than the sensitivity to $T_{\rm eff}$. The blue wing and central portion of Ly α were removed from the fit because the observed flux is very small in this region. Fig. 7 shows our best-fit model (red) compared to the solution using the $T_{\rm eff}$ value from Gianninas et al. (2011) in blue. The solution is clearly driven by the UV flux, and a $T_{\rm eff}$ value of 14,830 K, about 250 K larger than that of Gianninas et al. (2011), is required to fit the observations. The STIS photometric solution is added to Fig. 6 (dotted red line). It is reassuring that there is a good consistency between STIS spectrophotometry and white dwarf atmospheric parameters both for current hotter flux standards and this cooler object. A full discussion about using this white dwarf as a STIS spectrophotometric standard will be reported elsewhere. As an independent test, we have also used UBVRIJHK data drawn from Koen et al. (2010) and 2MASS (Cutri et al. 2003) to fit a temperature of 14,285 ± 900 K. The large error is due to the fact that this photometric data set does not include the UV which is the most sensitive to $T_{\rm eff}$. We refrain from using the *GALEX* FUV and NUV fluxes since there is a significant systematic offset between observed and synthetic fluxes in the magnitude range of WD 1327−083 (Camarota & Holberg 2014). The results are re-

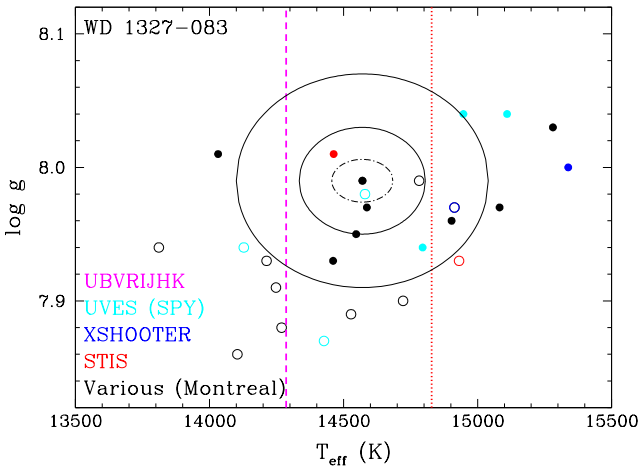

Figure 6. Characterisation of the atmospheric parameters for WD 1327−083 using different observations and model atmospheres. The standard atmospheric parameters from Gianninas et al. (2011) used throughout this work are represented by their 1σ and 2σ error ellipses (solid black). The smaller formal χ^2 error is represented by a dash-dotted ellipse. Different Balmer line solutions based on the same model atmospheres and fitting technique but alternative spectra are shown with solid circles. The alternative spectra are drawn from the Montreal group (black), the UVES instrument (SPY survey, cyan), X-SHOOTER (blue), and STIS spectrophotometry (red). We also show the alternative solutions employing the model atmospheres of Koester (2010) with open circles. The formal χ^2 error is very similar for all solutions. Finally, we show our best fits of the continuum flux of STIS spectrophotometry (dotted red, see Fig. 7) and UBVRIJHK photometry (dashed magenta, $\sigma_{\rm Teff} = 900$ K). For photometric fits we have fixed the surface gravity at $\log g = 8.0$.

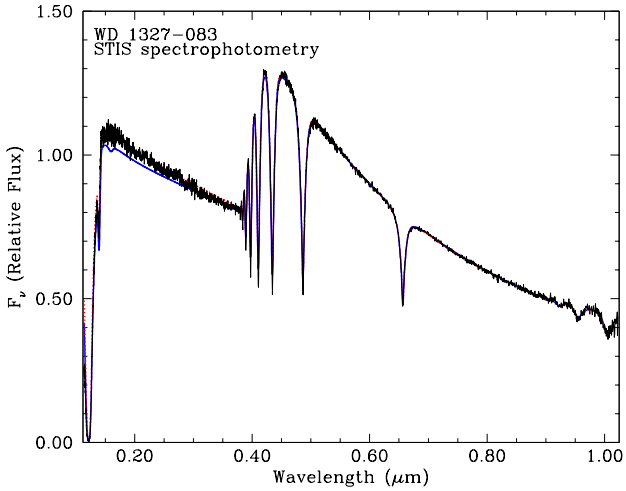

Figure 7. STIS spectrophotometric observations of WD 1327−083 as a function of wavelength. The predicted flux from the model atmospheres of Tremblay et al. (2011) using the atmospheric parameters of Gianninas et al. (2011) is shown in blue (solid, $T_{\rm eff} = 14,570$ K, $\log g = 7.99$), and the best fit is shown in red (dotted, $T_{\rm eff} = 14,830$ K with $\log g$ fixed at 8.0), which is almost coincident with the observations on this scale.

ported in Fig. 6 (dashed magenta), though because of the large error, the UBVRIJHK $T_{\rm eff}$ value is fully consistent with the STIS spectrophotometry.

Finally, we have performed the same analysis but using instead the model atmospheres of Koester (2010) including the Stark broadening profiles of Tremblay & Bergeron (2009). The results are shown in Fig. 6 with open circles for fits of the Balmer lines. The mean $T_{\rm eff}$ value is shifted by −295 K and the mean $\log g$ value by −0.06 dex, which is in both cases slightly larger than the published error bars. In the case of the STIS and UBVRIJHK photometric fits, we find essentially the same $T_{\rm eff}$ values with both grids of models.

Fig. 6 demonstrates that for the particular case of WD 1327−083, the 1σ error bars from Gianninas et al. (2011) are a reasonable but likely optimistic estimate of the $T_{\rm eff}$-$\log g$ uncertainties. It is perhaps not surprising since they did not consider alternative model grids or photometric solutions in their uncertainties. We have not explicitly considered the effect of the fitting techniques, which would increase even more the scatter between the different solutions. However, changing the fitting method would not provide a fully independent diagnostic since it is influenced by both the data reduction and systematic uncertainties in the model atmosphere grids.

It is outside the scope of this work to review the differences between the model grids or to re-observe spectroscopically all white dwarfs for which we currently have parallaxes. Nevertheless, we suggest that this should be done ahead of *Gaia* DR2 for a benchmark sample of bright white dwarfs. We can nevertheless make a few additional observations. If we allow the uncertainties on the atmospheric parameters to increase by a very conservative factor of two following our discussion above, 21/26 *Gaia* DR1 white dwarfs agree within error bars with thick H-layers while 22/26 are consistent with thin H-layers. These results suggest that given the precision on the atmospheric parameters, the theoretical MRR is entirely consistent with the observations. Furthermore, the distinction between thin and thick H-layers for *Gaia* DR1 white dwarfs is still out of reach, as it was the case for *Hipparcos*.

5 CONCLUSIONS

The *Gaia* DR1 sample of parallaxes was presented for 6 directly observed white dwarfs and 46 members of wide binaries. By combining this data set with spectroscopic atmospheric parameters, we have derived the semi-empirical MRR relation for white dwarfs. We find that, on average, there is a good agreement between *Gaia* parallaxes, published $T_{\rm eff}$ and $\log g$, and theoretical MRRs. It is not possible, however, to conclude that both the model atmospheres and interior models are individually consistent with observations. There are other combinations of $T_{\rm eff}$, $\log g$, and H envelope masses that could agree with *Gaia* DR1 parallaxes. However, the good agreement between observed and predicted radii for eclipsing binaries, which are insensitive to model atmospheres, suggest that both the atmospheric parameters and theoretical MRRs are consistent with *Gaia* DR1.

Starting with *Gaia* DR2, it will be feasible to derive the semi-empirical MRR for thousands of white dwarfs. Assuming systematic parallax errors will be significantly reduced, it will be possible to take advantage of large number statistics and compute a precise offset between the observed and predicted MRRs for $T_{\rm eff}$, mass, and spectral type bins. Alternatively, since the mass and radius are derived quantities, the parallax distances could be directly compared to predicted spectroscopic distances (Holberg et al. 2008). However, it may be difficult to interpret the results in terms of the precision of the model atmospheres and evolutionary models. Independent constraints from eclipsing binaries, as well as a more care-

ful assessment of the error bars for bright and well known white dwarfs, may still be necessary to fully understand *Gaia* data.

ACKNOWLEDGEMENTS

This project has received funding from the European Research Council (ERC) under the European Union's Horizon 2020 research and innovation programme (grant agreements No 677706 - WD3D and No 320964 - WDTracer). TRM is grateful to the Science and Technology Facilities Council for financial support in the form of grant No ST/L000733. This work has made use of data from the ESA space mission Gaia, processed by the Gaia Data Processing and Analysis Consortium (DPAC). Funding for the DPAC has been provided by national institutions, in particular the institutions participating in the Gaia Multilateral Agreement. The Gaia mission website is http://www.cosmos.esa.int/gaia. This work is based on observations made with the NASA/ESA Hubble Space Telescope, obtained at the Space Telescope Science Institute, which is operated by the Association of Universities for Research in Astronomy, Inc., under NASA contract NAS 5-26555. These observations are associated with programme #14213. This paper is based on observations made with ESO Telescopes under programme ID 097.D-0424(A).

REFERENCES

Althaus, L. G., Serenelli, A. M., & Benvenuto, O. G. 2001, MNRAS, 323, 471
Althaus, L. G., García-Berro, E., Isern, J., Córsico, A. H., & Rohrmann, R. D. 2007, A&A, 465, 249
Althaus, L. G., Córsico, A. H., Isern, J., & García-Berro, E. 2010a, A&ARv, 18, 471
Althaus, L. G., Córsico, A. H., Bischoff-Kim, A., et al. 2010b, ApJ, 717, 897
Althaus, L. G., Miller Bertolami, M. M., & Córsico, A. H. 2013, A&A, 557, A19
Andrews, J. J., Agüeros, M., Brown, W. R., et al. 2016, ApJ, 828, 38
Barstow, M. A., Bond, H. E., Holberg, J. B., et al. 2005, MNRAS, 362, 1134
Barstow, M. A., Bond, H. E., Burleigh, M. R., et al. 2015, in 19th European Workshop on White Dwarfs, ASP Conference Series, ed. P. Dufour, P. Bergeron & G. Fontaine (San Francisco: ASP), 493, 307
Bergeron, P., Saffer, R. A., & Liebert, J. 1992, ApJ, 394, 228
Bergeron, P., Leggett, S. K., & Ruiz, M. T. 2001, ApJS, 133, 413
Bergeron, P., Gianninas, A., & Boudreault, S. 2007, Proc. 15th European Workshop on White Dwarfs, ed. R. Napiwotzki & M. Burleigh (San Francisco, CA: ASP), 372, 29
Bergeron, P., Wesemael, F., Dufour, P., et al. 2011, ApJ, 737, 28
Bohlin, R. C., Gordon, K. D., & Tremblay, P.-E. 2014, PASP, 126, 711
Bond, H. E., Gilliland, R. L., Schaefer, G. H., et al. 2015, ApJ, 813, 106
Bours, M. C. P., Marsh, T. R., Gänsicke, B. T., & Parsons, S. G. 2015, MNRAS, 448, 601
Camarota, L., & Holberg, J. B. 2014, MNRAS, 438, 3111
Catalán, S., Isern, J., García-Berro, E., & Ribas, I. 2008, MNRAS, 387, 1693
Carrasco, J. M., Catalán, S., Jordi, C., et al. 2014, A&A, 565, A11
Casewell, S. L., Dobbie, P. D., Napiwotzki, R., et al. 2009, MNRAS, 395, 1795
Chandrasekhar, S. 1931, ApJ, 74, 81
Cohen, M., Megeath, S. T., Hammersley, P. L., Martín-Luis, F., & Stauffer, J. 2003, AJ, 125, 2645
Cummings, J. D., Kalirai, J. S., Tremblay, P.-E., Ramirez-Ruiz, E., & Bergeron, P. 2016, ApJ, 820, L18
Cutri, R. M., Skrutskie, M. F., van Dyk, S., et al. 2003, VizieR Online Data Catalog, 2246
Dobbie, P. D., Day-Jones, A., Williams, K. A., et al. 2012, MNRAS, 423, 2815
Falcon, R. E., Winget, D. E., Montgomery, M. H., & Williams, K. A. 2012, ApJ, 757, 116
Farihi, J., Burleigh, M. R., Holberg, J. B., Casewell, S. L., & Barstow, M. A. 2011, MNRAS, 417, 1735
Finley, D. S., & Koester, D. 1997, ApJ, 489, L79
Fontaine, G., Brassard, P., Bergeron, P., & Wesemael, F. 1992, ApJ, 399, L91
Fontaine, G., Brassard, P., & Bergeron, P. 2001, PASP, 113, 409
Gaia Collaboration, Brown, A. G. A., Vallenari, A., et al. 2016, arXiv:1609.04172
Giammichele, N., Bergeron, P., & Dufour, P. 2012, ApJS, 199, 29
Giammichele, N., Fontaine, G., Brassard, P., & Charpinet, S. 2016, ApJS, 223,
Gianninas, A., Bergeron, P., & Ruiz, M. T. 2011, ApJ, 743, 138
Gianninas, A., Dufour, P., Kilic, M., et al. 2014, ApJ, 794, 35
Girven, J., Gänsicke, B. T., Steeghs, D., & Koester, D. 2011, MNRAS, 417, 1210
Genest-Beaulieu, C., & Bergeron, P. 2014, ApJ, 796, 128
Goldsbury, R., Heyl, J., Richer, H. B., Kalirai, J. S., & Tremblay, P. E. 2016, ApJ, 821, 27
Gould, A., & Chanamé, J. 2004, ApJS, 150, 455
Greenstein, J. L. 1984, ApJ, 276, 602
Hamada, T., & Salpeter, E. E. 1961, ApJ134, 683
Hansen, B. M. S. 1999, ApJ, 520, 680
Hansen, B. M. S., Anderson, J., Brewer, J., et al. 2007, ApJ, 671, 380
Hansen, B. M. S., Richer, H., Kalirai, J., et al. 2015, ApJ, 809, 141
Harris, H. C., Dahn, C. C., Canzian, B., et al. 2007, AJ, 133, 631
Hermes, J. J., Brown, W. R., Kilic, M., et al. 2014, ApJ, 792, 39
Hintzen, P. 1986, AJ, 92, 431
Holberg, J. B., Wesemael, F., & Hubeny, I. 1984, ApJ, 280, 679
Holberg, J. B., Barstow, M. A., & Burleigh, M. R. 2003, ApJS, 147, 145
Holberg, J. B., & Bergeron, P. 2006, AJ, 132, 1221
Holberg, J. B., Bergeron, P., & Gianninas, A. 2008, AJ, 135, 1239
Holberg, J. B., Oswalt, T. D., & Barstow, M. A. 2012, AJ, 143, 68
Holberg, J. B., Oswalt, T. D., Sion, E. M., Barstow, M. A., & Burleigh, M. R. 2013, MNRAS, 435, 2077
Iben, I., Jr., & Tutukov, A. V. 1984, ApJ, 282, 615
Jordi, C., Gebran, M., Carrasco, J. M., et al. 2010, A&A, 523, A48
Kalirai, J. S., et al. 2008, ApJ, 676, 594
Kalirai, J. S. 2012, Nature, 486, 90
Kalirai, J. S., Marigo, P., & Tremblay, P.-E. 2014, ApJ, 782, 17
Karl, C. A., Napiwotzki, R., Heber, U., et al. 2005, A&A, 434, 637
Kawka, A., & Vennes, S. 2010, in Binaries - Key to Comprehension of the Universe, ASP Conference Series, ed. A. Prsa and M. Zejda (San Francisco: ASP), 435, 189
Kilic, M., Leggett, S. K., Tremblay, P.-E., et al. 2010, ApJS, 190, 77
Koen, C., Kilkenny, D., van Wyk, F., & Marang, F. 2010, MNRAS, 403, 1949
Koester, D., Schulz, H., & Weidemann, V. 1979, A&A, 76, 262
Koester, D. 1987, ApJ, 322, 852
Koester, D., Voss, B., Napiwotzki, R., et al. 2009, A&A, 505, 441
Koester D., 2010, Mem. Soc. Astron. Ital., 81, 921
Koester, D., & Kepler, S. O. 2015, A&A, 583, A86
Landolt, A. U., & Uomoto, A. K. 2007, AJ, 133, 768
Landolt, A. U. 2009, AJ, 137, 4186
Liebert, J., Bergeron, P., & Saffer, R.A. 1991, 7th European Workshop on White Dwarfs, NATO ASI Series, ed. G. Vauclair & E. M. Sion (Dordrecht: Kluwer), 409
Liebert, J., Bergeron, P., & Holberg, J. B. 2005, ApJS, 156, 47
Limoges, M.-M., Bergeron, P., & Lépine, S. 2015, ApJS, 219, 19
Lindegren, L., Lammers, U., Bastian, U., et al. 2016, arXiv:1609.04303
Marsh, M. C., Barstow, M. A., Buckley, D. A., et al. 1997, MNRAS, 286, 369
Maxted, P. F. L., Marsh, T. R., Moran, C. K. J., & Han, Z. 2000, MNRAS, 314, 334
McCook, G. P., & Sion, E. M. 1999, ApJS, 121, 1

Michalik, D., Lindegren, L., Hobbs, D., & Lammers, U. 2014, A&A, 571, A85
Michalik, D., Lindegren, L., & Hobbs, D. 2015, A&A, 574, A115
Nagel, T., Schuh, S., Kusterer, D.-J., et al. 2006, A&A, 448, L25
Oswalt, T. D., & Strunk, D. 1994, Bulletin of the American Astronomical Society, 26, 28.09
O'Brien, M. S., Bond, H. E., & Sion, E. M. 2001, ApJ, 563, 971
Parsons, S. G., Marsh, T. R., Copperwheat, C. M., et al. 2010, MNRAS, 402, 2591
Parsons, S. G., Marsh, T. R., Gänsicke, B. T., et al. 2012b, MNRAS, 420, 3281
Parsons, S. G., Gänsicke, B. T., Marsh, T. R., et al. 2012c, MNRAS, 426, 1950
Parsons, S. G., Marsh, T. R., Gänsicke, B. T., et al. 2012a, MNRAS, 419, 304
Parsons, S. G., Hill, C. A., Marsh, T. R., et al. 2016, MNRAS, 458, 2793
Perlmutter, S., et al. 1999, ApJ, 517, 565
Perryman, M. A. C., de Boer, K. S., Gilmore, G., et al. 2001, A&A, 369, 339
Provencal, J. L., Shipman, H. L., Høg, E., & Thejll, P. 1998, ApJ, 494, 759
Pyrzas, S., Gänsicke, B. T., Brady, S., et al. 2012, MNRAS, 419, 817
Riess, A. G., et al. 1998, AJ, 116, 1009
Romero, A. D., Córsico, A. H., Althaus, L. G., et al. 2012, MNRAS, 420, 1462
Romero, A. D., Kepler, S. O., Córsico, A. H., Althaus, L. G., & Fraga, L. 2013, ApJ, 779, 58
Salaris, M., Cassisi, S., Pietrinferni, A., Kowalski, P. M., & Isern, J. 2010, ApJ, 716, 1241
Schmidt, H. 1996, A&A, 311, 852
Shipman, H. L. 1979, ApJ, 228, 240
Shipman, H. L., Provencal, J. L., Høg, E., & Thejll, P. 1997, ApJ, 488, L43
Silvestri, N. M., Oswalt, T. D., & Hawley, S. L. 2002, AJ, 124, 1118
Sion, E. M. 1984, ApJ, 282, 612
Subasavage, J. P., Jao, W.-C., Henry, T. J., et al. 2009, AJ, 137, 4547
Tokovinin, A., & Lépine, S. 2012, AJ, 144, 102
Torres, S., García-Berro, E., Isern, J., & Figueras, F. 2005, MNRAS, 360, 1381
Tremblay, P.-E., & Bergeron, P. 2008, ApJ, 672, 1144
Tremblay, P.-E., & Bergeron, P. 2009, ApJ, 696, 1755
Tremblay, P.-E., Bergeron, P., & Gianninas, A. 2011, ApJ, 730, 128
Tremblay, P.-E., Ludwig, H.-G., Steffen, M., & Freytag, B. 2013, A&A, 559, A104
Tremblay, P.-E., Kalirai, J. S., Soderblom, D. R., Cignoni, M., & Cummings, J. 2014, ApJ, 791, 92
Tremblay, P.-E., Gianninas, A., Kilic, M., et al. 2015, ApJ, 809, 148
van Altena, W. F., Lee, J. T., & Hoffleit, E. D. 1994, The General Catalogue of Trigonometric Parallaxes (New Haven: Yale University Observatory)
van Leeuwen, F. 2007, A&A, 474, 653
Vauclair, G., Schmidt, H., Koester, D., & Allard, N. 1997, A&A, 325, 1055
Vennes, S., Thejll, P. A., Génova Galvan, R., & Dupuis, J. 1997, ApJ, 480, 714
Weidemann, V. 2000, A&A, 363, 647
Werner, K. 1996, ApJ, 457, L39
Williams, K. A., Bolte, M., & Koester, D. 2009, ApJ, 693, 355
Wood, M. A. 1995, in 9th European Workshop on White Dwarfs, ed. D. Koester & K. Werner (Springer: Berlin), 41
Zacharias, N., Finch, C. T., Girard, T. M., et al. 2012, VizieR Online Data Catalog, 1322
Zuckerman, B., Xu, S., Klein, B., & Jura, M. 2013, ApJ, 770, 140
Zuckerman, B. 2014, ApJ, 791, L27

This paper has been typeset from a TEX/LATEX file prepared by the author.